ELSEVIER

Journal of Alloys and Compounds 458 (2008) 248–252

Journal of ALLOYS AND COMPOUNDS

www.elsevier.com/locate/jallcom

Mechanochemical effects on microstructure and transport properties of nanocrystalline $La_{0.8}Na_{0.2}MnO_3$ ceramics

Tao Wang [a], Xiaodong Fang [a,*], Weiwei Dong [a], Ruhua Tao [a], Zanhong Deng [a], Da Li [a], Yiping Zhao [a], Gang Meng [a], Shu Zhou [a], Xuebin Zhu [b]

[a] *Anhui Institute of Optics and Fine Mechanics, Chinese Academy of Sciences, Hefei 230031, PR China*

[b] *Key Laboratory of Materials Physics, Institute of Solid State Physics, Chinese Academy of Sciences, Hefei 230031, PR China*

Received 10 February 2007; received in revised form 3 April 2007; accepted 4 April 2007

Available online 8 April 2007

Abstract

Mechanochemical effects on microstructure and transport properties of the sol–gel prepared nanocrystalline $La_{0.8}Na_{0.2}MnO_3$ ceramics have been studied. It was found that with the prolonging of the milling time the crystalline size as well as the particle size obviously decreased while the resistivity increased. The strain of the milled samples was calculated using the Williamson–Hall plot, which increased with the increase of the milling time. The surface layer with large defects and the strain led to the decrease of the insulator-metal transition temperature, but the magnetoresistance value within the whole measured temperature range of 80–300 K was remarkably improved, which indicated that it was an effective route to enhance the magnetoresistance value both at low temperature and at high temperature by mechanochemical processing.

Keywords: Ceramics; Mechanochemical processing; Electrical transport

1. Introduction

The observations of the colossal magnetoresistance (CMR) effects in the perovskite manganites have attracted much attention because of their rich physical properties and potential applications such as magnetic field sensors, memory cells [1–4]. The double-exchange (DE) mechanism proposed by Zener [5], the Jahn–Teller (JT) polaron [6], the tolerance factor (t) [7] and the phase separation [8] have been used to interpret the properties of the manganites. In the DE system, the insulator-metal (IM) transition temperature (T_{IM}) always coincides with the paramagnetic–ferromagnetic (PM–FM) transition temperature (T_c). With the applied field, the T_{IM} as well as the T_c shifts to higher temperatures, and the resistivity largely decreases resulting in the CMR phenomena. Until now, two types of magnetoresistance (MR) have been recognized in the manganese oxides, the intrinsic MR induced by the DE between the Mn^{3+}–O–Mn^{4+} and the extrinsic MR induced by the tunneling effects between the grain boundaries (GBs) [9]. Moreover, it is suggested that large low-field MR (LFMR) can be obtained when the crystalline size is decreased to nanoscale, which is interesting for physical researches as well as for potential applications [10–22].

So far, the previous works have mainly focused on the manganites doped with divalent elements such as Ca, Sr, Ba and Pb, but there are only a few reports on the magnetic and transport properties of monovalent element-doped manganites. Unlike divalent element-doped manganites, the monovalent element-doped manganites have some interesting features. One of the most important features is that it is possible to achieve an equal amount of holes with a lower cation substitution for La sites, which will result in lower cation disorder [23,24]. In the monovalent element-doped manganites, the $La_{1-x}Na_xMnO_3$ is a typical system and it has relatively large MR values near room temperature [23–27].

It is well known that mechnochemical method is an effective route to prepare the nanocrystal ceramics, which has been used to prepare various nanocrystal materials including manganese oxides [13,16,19,20]. As for the $La_{1-x}Na_xMnO_3$ ceramics, there have no relative reports about the mechanochemical effects on the microstructures as well as on the properties. In this letter, nanocrystalline $La_{0.8}Na_{0.2}MnO_3$ (LNMO) ceramics were pre-

* Corresponding author. Tel.: +86 551 5593508; fax: +86 551 5593527.
E-mail address: xdfang@aiofm.ac.cn (X. Fang).

0925-8388/$ – see front matter © 2007 Elsevier B.V. All rights reserved.
doi:10.1016/j.jallcom.2007.04.023

pared by the sol–gel method, and the ball milling was used to further decrease the crystalline size. It was observed that the mechnochemical effects played very important roles on the microstructures and properties of the LNMO ceramics.

2. Experimental procedure

The LNMO ceramics were prepared by the sol–gel method. The raw materials were La_2O_3, $Na(CH_3COO)$, and MnO_2. The citric acid (CA) was used as chelate. First, stoichiometric La_2O_3 and $Na(CH_3COO)$ were dissolved in diluted nitric acid, and then MnO_2 was added into the above solution. In order to dissolve the MnO_2 completely, appropriate H_2O_2 was added and finally transparent solution was obtained. The solution was stirred for 10 h using magnetic stirrer in order to get well-mixed solution. The solution was firstly dried at 373 K, and then dried at 573 K in order to expel the organics. The resulting powders were calcined at 1073 K for 24 h in air, and then the powders were pressed into four pellets and sintered at 1173 for 12 h in air. Afterwards, three pellets were crushed into powders in an agate mortar, and milled with different time using a planetary ball miller, and finally pressed again into pellets and calcined at 973 K for 2 h in air. For the sake of description, the samples milled with 0, 5, 10 and 20 h are defined as the sample MA0, MA5, MA10 and MA20, respectively.

A Philips X'pert PRO X-ray diffractometer (XRD) with Cu Kα and a FEI designed Sirion 200 field-emission scanning electron microscopy (FE-SEM) were used to characterize the composition and the microstructure. The temperature dependence of the resistivity under the applied fields of 0 and 0.5 T was measured by the standard four-probe method by means of cryogenic refrigeration equipment. The MR was defined as $MR\ (\%) = [(\rho_0 - \rho_H)/\rho_0] \times 100$, where ρ_0 and ρ_H are the resistivities under zero field and an applied field, respectively.

3. Results and discussion

Fig. 1 is the XRD θ–2θ results for the different LNMO samples. The structure can be indexed with rhombohedral and the space group is R-3c. With the increase of the milling time, the full width at half maximum (FWHM) increases for all diffraction peaks within the measurement range. Moreover, it can be seen that as the milling time increases from 0 to 5 h, all the splitted diffraction peaks are incorporated into a single one because of the broadening of diffraction peaks. In most cases, line broadening occurs due to simultaneous size and strain effects. Since the ball milling introduces considerable strain in the samples, the contribution of strain to the diffraction line broadening is not negligible. The decrease of the crystalline size and the induced strain effects should be considered simultaneously [19,20].

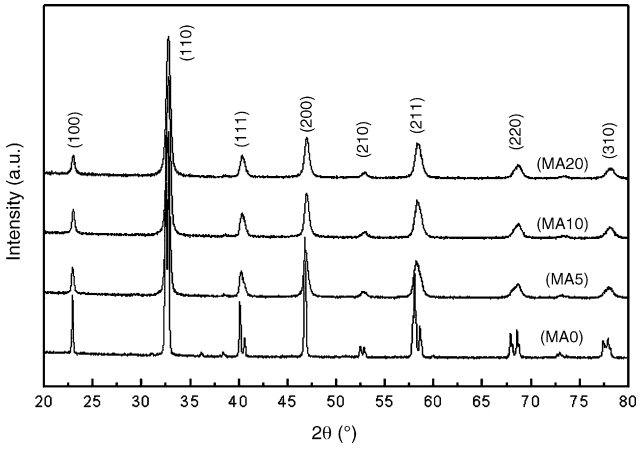

Fig. 1. XRD results of LNMO samples milled with different time.

One of the effective routes to separate the above two effects is known as the Williamson–Hall plot [19], which can be expressed as follows:

$$B \cos \theta = \frac{K\lambda}{D} + 2\varepsilon \sin \theta \quad (1)$$

where B is the FWHM of the XRD peaks and K the Scherrer constant, D the crystalline size, λ the wavelength of the X-ray, ε the lattice strain, and θ is the Bragg angle.

For the Gaussian X-ray profiles, B can be calculated as follows:

$$B^2 = B_m^2 - B_s^2 \quad (2)$$

where B_m is the FWHM for the measured sample and B_s is the FWHM of the standard sample. Here, the sample MA0 is selected as the standard sample.

In the plot of $B\cos\theta$ (y-axis) versus $2\sin\theta$ (x-axis), a linear fitting is used, and the intercept of the y-axis gives the crystalline size D and the slope gives the strain ε.

The milling effects on the crystalline size and the strain are shown in Fig. 2(a) and (b), respectively. From Fig. 2(a), it can be clearly seen that with the increase of the milling time from 5 to 10 h the crystalline size is decreased rapidly from 44 to 17 nm, but the tendency slows down as the milling time further increases. The crystalline size obtained through 20 h milling processing is 14 nm. The reason can be attributed to that with the

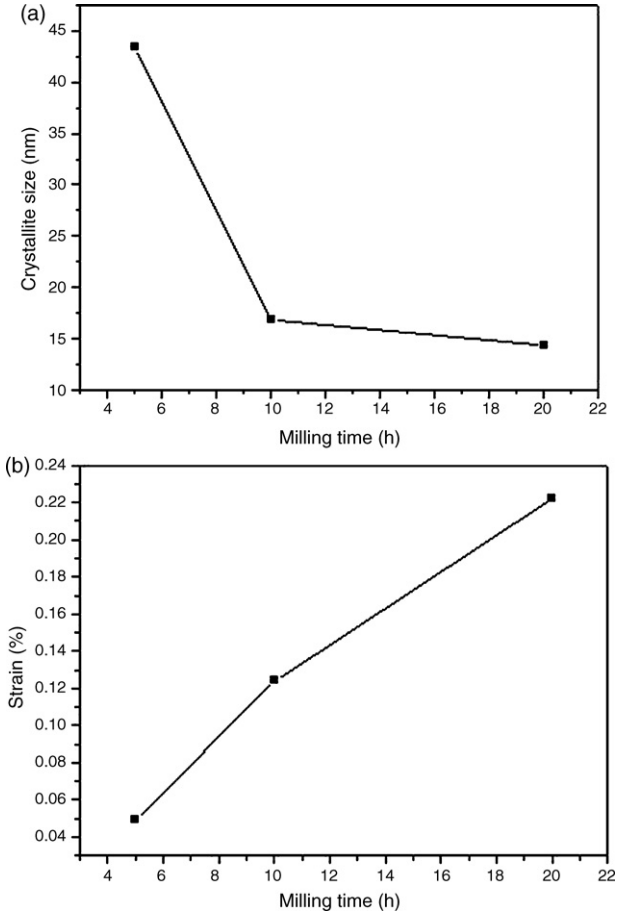

Fig. 2. Milling time dependence of crystalline size (a) and strain (b).

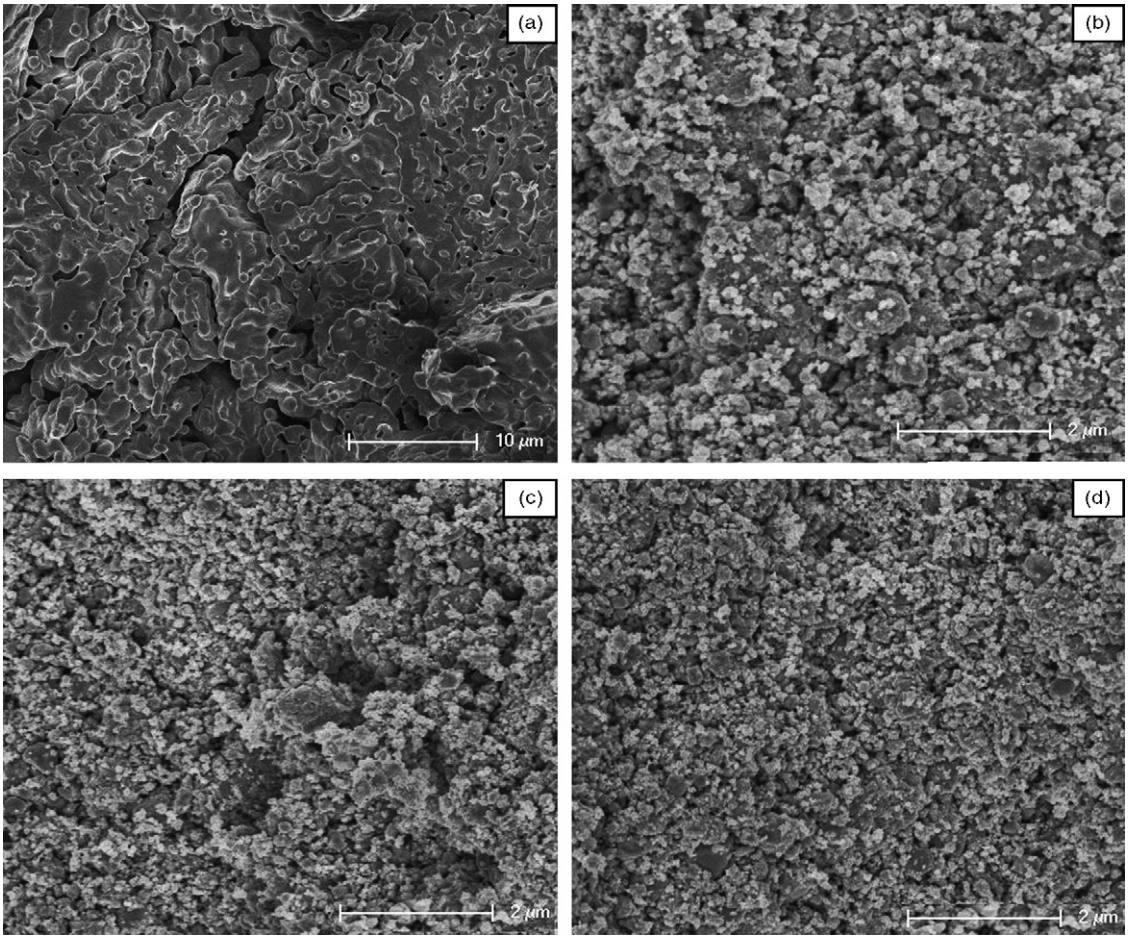

Fig. 3. FE-SEM results of the LNMO milled with different time (a) MA0; (b) MA5; (c) MA10; (d) MA20.

decrease of the crystalline size the strain will harden the powders, which makes it difficult to further decrease the crystalline size [16]. As shown in Fig. 2(b), it can be obviously seen that the strain is largely increased with the increase of the milling time, which may be attributed to the introduction of large amounts of defects in the ceramics [16].

Fig. 3 is the FE-SEM results of the LNMO samples. It can be seen that the sample MA0 is dense and the particle size is homogenous; however, for the milled samples, with the increase of the milling time more and more small particles are introduced, which will result in the decrease of the particle size.

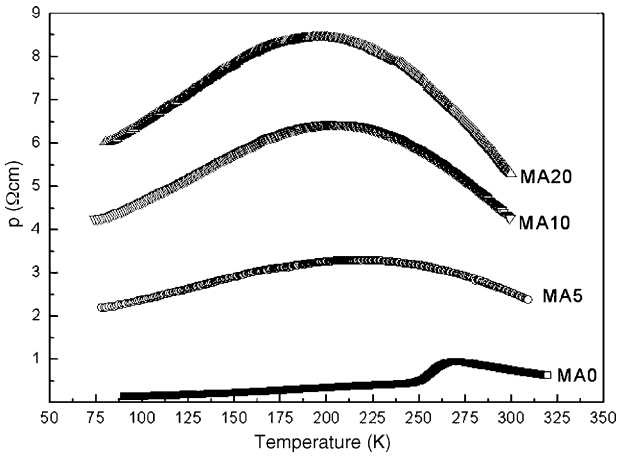

Fig. 4. ρ-T results for different LNMO samples under 0 T.

Fig. 4 is the results of ρ–T for all the samples under 0 T, and the detailed electrical transport parameters are listed in Table 1. It can be seen that all the samples show an IM transition, which can be well explained by the DE [5]. Moreover, as the milling time increases, the T_{IM} is decreased and the resistivity is continuously increased, which can be attributed to the decrease of the crystalline size [11,12,20,21]. From Table 1, it can be observed that the T_{IM} of the sample MA0 is about 270 K, which is lower than that of the previously reports and it may be related to the smaller crystalline size in our experiment [23–27]. As for the origin of the decrease of the T_{IM} and the increase of the resistivity, the reason is discussed as follows. It is recognized that when the crystalline size is reduced to tens of nanometers the man-

Table 1
Detailed parameters for the transport properties

Sample	T_{IM} (K)	ρ (T_{IM}) (Ω cm)
MA0	269.8	0.94
MA5	220.4	3.29
MA10	200.5	6.45
MA20	197.3	8.45

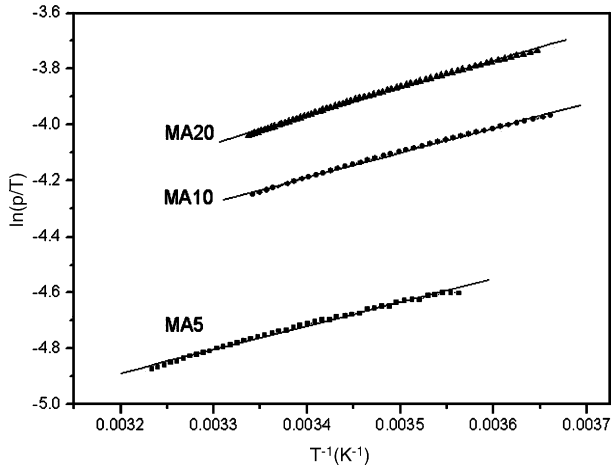

Fig. 5. $\ln(\rho/T)$ vs. T^{-1} results for the samples MA5, MA10 and MA20, and the solid lines are the fitting results using the SPH model.

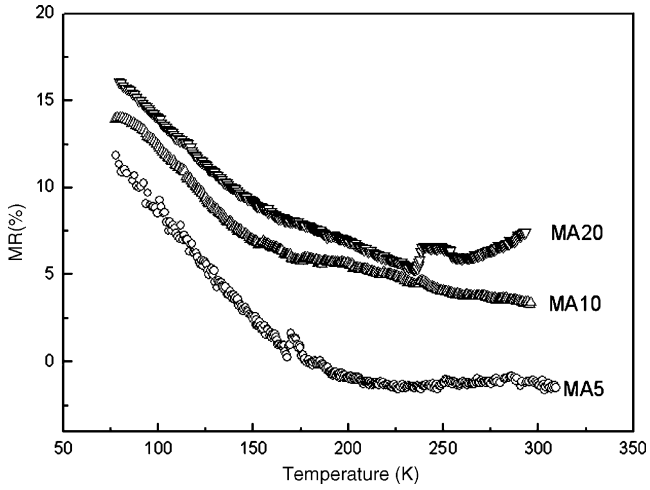

Fig. 6. MR–T for the milled samples.

ganites grains can be considered as a two-phase system, which are composed of a core phase and a surface layer [20,21]; the core phase has the same properties with the bulk, but the surface layer has lots of defects such as the oxygen nonstoichiometry, the broken Mn^{3+}–O–Mn^{4+} bonds, the faults of the crystallographic structure and dislocations. Additionally, when the milling time is increased, the crystalline size is decreased that will lead to the enhancement of the surface layer volume. The surface layer with large amounts of defects will block the carrier transition, which will result in the decrease of T_{IM} and the increase of the resistivity. Moreover, from Fig. 2(b), it can be observed that the strain is obviously increased with the increase of the milling time. The increase of the strain can aggravate the distortion of the MnO_6 octahedron, which will also lead to the decrease of the T_{IM} and the increase of the resistivity.

As for the conduction mechanism above the temperature T_{IM}, three possible models can be used, the conventional thermal activation (TA) model with $\rho = A\exp(E_a/K_BT)$, the small polaron hopping (SPH) model with $\rho = BT\exp(E_a/K_BT)$ and the variable range hopping model (VRH) with $\rho = \rho_0\exp(T_0/T)^{1/4}$. In all these models, K_B is the Boltzmann constant and E_a is the activation energy. In our experiments, it is found that only the SPH model can be well used, and the results are shown in Fig. 5. The detailed fitting parameters are listed in Table 2. It can be observed that the activation energy E_a is continuously increased with the increase of the milling time, which can be attributed to the introduction of large amounts of defects.

The temperature dependence of MR for all the milled samples under 0.5 T within the temperature range of 80–300 K is shown in Fig. 6. It can be seen that the MR increases with the decrease of temperature. With the increase of the milling time, the MR value is obviously increased. Commonly, it can be found that the intrinsic MR near the T_{IM} is decreased or unchanged with the decrease of the crystalline size, but the MR at low temperature can be largely improved with the decrease of the crystalline size due to the intergrain spin-polarized tunneling across the grain boundaries [9]. As for our experiments, the milling process makes the decrease of the grains and the increase of the MR near the T_{IM}, which suggests that the strain introduced by the milling process is a key factor to alter the properties of the as-prepared samples, and it will be systematically studied in the following investigations.

Table 2
Activation energy obtained from SPH model

Sample	Activation energy, E_a (meV)
MA5	72.64
MA10	77.58
MA20	85.69

4. Conclusions

In summary, mechanochemical effects on microstructure and transport properties of the sol–gel prepared nanocrystalline $La_{0.8}Na_{0.2}MnO_3$ ceramics have been studied. The crystalline size and the T_{IM} are decreased, and the resistivity is increased with the prolonging of the milling time, which can be attributed to the expansion of the surface layer volume and the increase of the strain. The magnetoresistance value within the whole measured range of 80–300 K was obviously improved, which indicates that it is effective to enhance the magnetoresistance both at low temperatures and at high temperatures by mechanochemical process.

Acknowledgments

Financial support from the Director's Fund of Hefei Institutes of Physical Science, Chinese Academy of Sciences and from the Chinese Academy of Sciences under the Program for Recruiting Outstanding Overseas Chinese (Hundred Talents Program) is gratefully acknowledged.

References

[1] R. von Helmolt, J. Wecher, B. Holzapfel, L. Schultz, K. Samwer, Phys. Rev. Lett. 71 (1993) 2331.

[2] S. Jin, T.H. Tiefel, M. McCormack, R.A. Fastnacht, R. Ramesh, L.H. Chen, Science 264 (1994) 413.
[3] A. Asamitsu, Y. Moritomo, Y. Tomioka, T. Arima, Y. Tokura, Nature 373 (1995) 407.
[4] J.M.D. Coey, M. Viret, S. von Molnar, Adv. Phys. 48 (1999) 167.
[5] C. Zener, Phys. Rev. 82 (1951) 403.
[6] E. Dagotto, T. Hotta, A. Moreo, Phys. Rep. 344 (2001) 1–153.
[7] J. Fontcuberta, B. Martinez, A. Seffar, S. Pinol, et al., Phys. Rev. Lett. 76 (1996) 1122.
[8] A.J. Millis, B.I. Shraiman, R. Mueller, Phys. Rev. Lett. 77 (1996) 175.
[9] H.Y. Hwang, S.W. Cheong, N.P. Ong, B. Batlogg, Phys. Rev. Lett. 77 (1996) 2041.
[10] S.L. Yuan, M.H. Liu, Z.Y. Li, G. Peng, et al., Solid. State. Commun. 121 (2002) 291.
[11] L.W. Lei, Z.Y. Fu, J.Y. Zhang, Mater. Lett. 60 (2006) 970.
[12] A. Gaur, G.D. Varma, J. Phys.: Condens. Matter. 18 (2006) 8837.
[13] I. Panagiotopoulos, N. Moutis, M. Ziese, A. Bollero, J. Magn. Magn. Mater. 299 (2006) 94.
[14] A. Dutta, N. Gayathri, R. Ranganathan, Phys. Rev. B 68 (2003) 054432.
[15] A.K.M. Akther Hossian, L.F. Cohen, F. Damay, et al., J. Magn. Magn. Mater. 192 (1999) 263.
[16] S. Roy, I. Dubenko, D.D. Edorh, N. Ali, J. Appl. Phys. 96 (2004) 1202.
[17] S.L. Patil, A.S. Ogale, S.R. Shinde, D.C. Kundaliya, et al., J. Appl. Phys. 97 (2005) 10H707.
[18] G. Venkataiah, D.C. Krishna, M. Vithal, S.S. Rao, et al., Physica B 357 (2005) 370.
[19] P. Kameli, H. Salamati, A. Aezami, J. Appl. Phys. 100 (2006) 053914.
[20] P. Kameli, H. Salamati, A. Aezami, J. Alloy compd. (2006) doi:10.1016/j.jallcom.2006.10.078.
[21] P. Dey, T.K. Nath, Phys. Rev. B 73 (2006) 214425.
[22] P. Dey, T.K. Nath, U. Kumae, P.K. Mukhopadhyay, J. Appl. Phys. 98 (2005) 014306.
[23] L. Malavasi, M.C. Mozzati, I. Alessandri, M. Affronte, V. Cervetto, C.B. Azzoni, G. Flor, Solid State Ionics 172 (2004) 265.
[24] M. Sahana, R.N. Singh, C. Shivakumara, N.Y. Vasanthacharya, M.S. Hegde, Appl. Phys. Lett. 70 (1997) 2909.
[25] W.W. Dong, X.B. Zhu, R.H. Tao, X.D. Fang, J. Crystal Growth 290 (2006) 180.
[26] X.B. Zhu, J. Yang, B.C. Zhao, Z.G. Sheng, S.M. Liu, W.J. Lu, W.H. Song, Y.P. Sun, J. Phys. D: Appl. Phys. 37 (2004) 2347–2351.
[27] X.B. Zhu, Z.G. Sheng, S.M. Liu, J. Yang, B.C. Zhao, W.J. Lu, W.H. Song, J.M. Dai, Y.P. Sun, Phys. B: Condens. Matter. 364 (2005) 43.